Design and analysis of PZT micropumps for biomedical applications: Glaucoma treatment

Mustafa Zahid Yildiz* and Hamid Asadi Dereshgi**

*Department of Electrical & Electronics Engineering, Faculty of Technology, Sakarya University of Applied Sciences, Sakarya, Turkey
** Mechatronics Engineering, Institute of Natural Sciences, Sakarya University, Turkey
*Corresponding Author: mustafayildiz@sakarya.edu.tr

ABSTRACT

Micropumps have wide range of novel applications in medical field. The main purpose of this study was to find potential electro-mechanical design aspects of a micropump for Glaucoma disease treatment. We suggested four new micropump designs, namely, single diaphragm micropumps at two different Piezoelectric Lead Zirconate Titanate (PZT-2) thicknesses, a bi-diaphragm micropump, and a peristaltic micropump. The driving voltage values in the simulations were 5 V to 45 V by 5 V increments and the frequencies were 5 Hz and 10 Hz. Two dimensional analyses were done with COMSOL Multiphysics 4.3. Three different one-way Analysis of Variance (ANOVA) analyses were performed to find out the effect of voltage and frequencies on flow rates. At different frequencies, there were significant differences in flow rates and fluid pressures ($p < 0.05$) for each micropump design. At different driving voltages, flow rates, displacement values, and fluid pressures were statistically different ($p < 0.001$) for all micropumps. The maximum flow rate obtained in peristaltic micropump was 1.62×10^{-27} m³/cycle. The maximum displacement of diaphragm occurred in bi-diaphragm micropump was 3.68×10^{-3} mm, which was obtained at 45 V and 5 Hz. According to our result, peristaltic micropump design might be used for glaucoma treatment.

Keywords: Micropump design, nozzle/diffuser elements, PZT-2 actuation, COMSOL Multiphysics.

INTRODUCTION

Glaucoma enters irreversible damage to the optic nerves and causes reduced vision and eventually blindness. The Glaucoma disease has several types that are all leading to blindness. Gradual decline in vision bring personal and social costs. For this reason, it will have a serious impact on quality of life. Glaucoma is a serious threat to all people in the world (De Moraes et al., 2017; McMonnies et al., 2017). In the treatment of this disease, there are certain techniques such as eye drops (Schuettauf et al., 2002), surgery (Elder, M. J. 1994), and shunt devices that are used (Lloyd et al., 2001). These techniques try to drop intraocular pressure below a certain value. Thus, micropumps can be useful to control this important pressure level.

The shunt device is implanted into the eye. Shunts flow out the aqueous humour that is a clear fluid between the cornea and lens, from the anterior chamber (part of area containing the aqueous humour of the eye in front of iris) to an evacuated chamber with lower pressure resulting in reduced intraocular pressure. Unfortunately, sometimes shunt devices make biological contamination and growth of scar tissue that increases flow resistance. For this reason, in the treatment of Glaucoma disease with shunt devices, there is a possibility that the intraocular pressure may rise again (Kawun et al., 2016).

Nowadays, we can see significant development in drug delivery devices based on Micro-Electro-Mechanical-Systems (MEMS) technology. Conventional drug delivery methods such as tablets and immediate delivery drugs by syringes are not always effective (Nisar et al., 2008). Microfluidics is ever increasing requirements of medical industry. In this area, the basic need for microfluidic device that can sense, mix, pump, and control in small volume

is an important requirement (Nisar et al., 2008). Thereby, micropumps are called beating heart of microfluidics. Micropumps from the early years of the development of micro-electromechanical systems have been considered by researchers (Wang et al., 2018). Drug delivery with high accuracy and low cost always has been one of the goals of micropump designers. Among the first micropumps in the literature, the designed micropump by Jan G. Smits in 80s to use in controlled insulin transmission system to diabetic patients was used (Smits, 1990). In diabetics, large volume injection of the drug into the body is not used. A diabetic patient needs less than one milliliter of insulin each day. For this reason, micropumps may play important roles in the treatment of this disease.

Heidi Gensler et al. (2012) designed a micropump for drug delivery for small animals such as mice for the first time. The small amount of drug was delivered by time control circuits of the micropump (Gensler et al., 2012).

Paul Braineard Eladi et al. (2014) designed and produced a valveless micropump with PZT actuator. In their design, three distinct layers were used consisting of two layers of silicon and a layer of glass. These three layers were covered on top of each other and a composite structure was created. Water and methanol fluid were selected for pumping process. They examined the effects of nozzle/diffuser, micropump chamber height, voltage, and frequency of the vibrating diaphragm elements of the net flow rate. For this micropump, the ideal voltage and frequency were achieved at 80 V and 250 Hz, respectively. In the ideal condition of pumping process, back pressure for water was zero and for methanol, 360 Pa (Eladi et al., 2014).

Angelica Cobo et al. (2016) offered a wireless micropump with a capability of being implanted in the small animal's body. The purpose of this micropump design was chronic drug delivery and development of cancer treatment. This micropump was tested for 30 days and had the 30 µl daily production capability. During this time, the resulting error rate was expressed to be less than 4 % (Cobo et al., 2016).

In this current study, four novel micropumps with Piezoelectric Lead Zirconate Titanate (PZT-2) diaphragms were designed and investigated numerically. These micropumps consisted of the chamber, the silicon membrane, PZT, and two micro-valves without moving parts. In order to be used in biomedical applications, the applied voltage to PZT vibration was considered less than 45 V, which might be biologically convenient in many cases. The effects of voltage and frequency of the excitation input of the four micropumps on net flow rates, displacements, and fluid pressures were measured. ANOVA analyses showed statistically significant difference in flow rate and fluid pressure ($p < 0.05$). Peristaltic micropump showed superior net-flow performance when considered similar voltage and frequency values. In this way, peristaltic micropump design may be the best candidate for glaucoma treatment among others.

MATERIALS AND METHODS

Micropumps can have a significant role in controlling and injection of drug dose. In this section, four new designs of valveless micropumps were provided and evaluated, namely, single diaphragm micropump (SDM), bi-diaphragm micropump (BDM), and peristaltic micropump (PSM). The micropumps design was presented in Figure 1. Their analysis was performed in two-dimensional mode. Except for the diaphragms, other parameters of micropumps were exactly equal. The geometry and micropump dimensions were chosen based on the fabrication technology and their applications in medical area. The micropump chamber dimensions were 25 mm × 4 mm, the divergence angle of the micro-valves of nozzle/diffuser was 10° and the length of these elements was 10.2870 mm and the dimension of silicon membrane was 25 mm × 0.1 mm. Diaphragm's actuator was made of PZT. In the SDMs, the PZT thicknesses were 200 µm and 250 µm with fixed length of 14 mm. In BDM, two PZT were located parallel to each other. In fact, the bottom wall of SDM chamber was removed and a second diaphragm was installed to create BDM. PZT dimensions for this micropump were 14 mm × 0.2 mm. Additionally, in PSM, four PZT and two parallel diaphragms were used. On each diaphragm, there were two serial PZT actuators. The dimensions of designed PZT for this micropump were 7 mm × 0.2 mm.
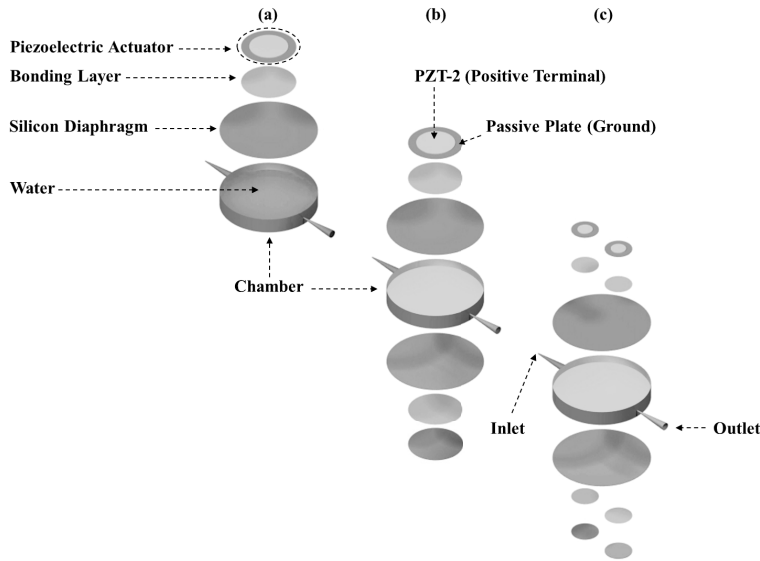
Fig. 1. Exploded view of the micropumps: (a) SDM, (b) BDM, and (c) PSM.

The excitation voltage was applied to the PZT-2 actuator. Positive terminal of sinusoidal voltage source was connected to the center of the PZT disk; ground terminal was connected to the passive plate.

WORKING PRINCIPLE

The silicon membrane separates the fluid of micropump chamber from the PZTs. We applied sinusoidal voltage to the PZTs. In effect of sinusoidal voltage, longitudinal expansion and contraction took place in PZT. Amplitude of the vibration was much smaller than length of the PZT. By connecting the PZT to the silicon membrane, the longitudinal expansion and contraction are converted to the transverse mode. As a result, the fluid is transferred from the reservoir to the chamber and from the chamber to the outside. The applied voltages were sinusoidal 5 V to 45 V by 5 V increments, and frequencies were 5 Hz and 10 Hz. The voltage determines the amplitude of the diaphragm vibration and the frequency determines the numbers of displacement in time. The optimal frequency may vary according to the material and dimension of the PZT. If the frequency is not selected properly, the pumping rate will be reduced. Because the diaphragm cannot reach the peak point of displacement, the amplitude of the displacement will be reduced (Fan et al., 2004). The flow rate can be calculated from Equation (1) (Lee et al., 2016).

$$Flow\,rate = \frac{frequency}{Number\,of\,Electrods} \times \frac{flow\,rate}{cycle} \tag{1}$$

Diaphragms to generate net flow rate need a diodicity method. Diaphragm displacement profiles are usually symmetric. This issue causes non-directional flow. Hence, the micro-valves are used for transforming the non-directional flow rate to directional one. In the period that the diaphragm is bent towards the fluid inside the chamber, a greater volume of fluid in the chamber can be guided in one direction to the outside. High flow rate, high back pressure of fluid, and lower power consumption are the features that are considered in an ideal micropump (Shabanian et al., 2016).

Micro-valves are classified as either valve or valveless types depend on the structure of them (Ma et al., 2016; Jenke et al., 2018). Micropumps with check valve, we face with problems such as detrition of moving valves, sensitivity to the solid particles, pressure loss (Cui et al., 2008). Micropumps with check valves can prevent of back flow, but the structure of pump is complicated. Also, there is the blocking risk of valve by small particles or bubbles of fluid (Revathi et al., 2018). In other words, bilateral mode of micro-valves of nozzle/ diffuser does not completely prevent the back

flow. In these micro-valves the shape and divergence angle can be important and influencing on the performance of the pumps (Aggarwal et al., 2017; Yang et al., 2015).

In BDM, we applied opposite voltages to PZT actuator. In other words, the PZT vibrates in the opposite directions. In this way, in the positive alternation of the sinusoidal signal where the suction takes place, the micropump chamber becomes larger and more fluid transfer from the reservoir to the chamber, whereas, in the negative alternation of the sinusoidal signal, the discharge phenomena occur. Both diaphragms are bent into the chamber and the chamber volume is decreased. In this case, the fluid pressure inside the chamber will be increased.

The working principle of PSM, in fact, is like BDM. PZT actuators that are parallel to each other because of opposite pressure vibrate in the opposite direction to each other. Also, opposite voltage is applied to the two PZT that are connected on a common silicon membrane. In fact, the micropump chamber is divided into two halves. Two PZT that in the left hand of chamber are parallel to each other and are in the state of discharge period. In the same period the right handed PZT of chamber creates a suction mode on diaphragm. Hence, the fluid in the chamber with peristaltic mode is guided to the output micro-valve. Figure 2 shows the principle of proposed micropumps.
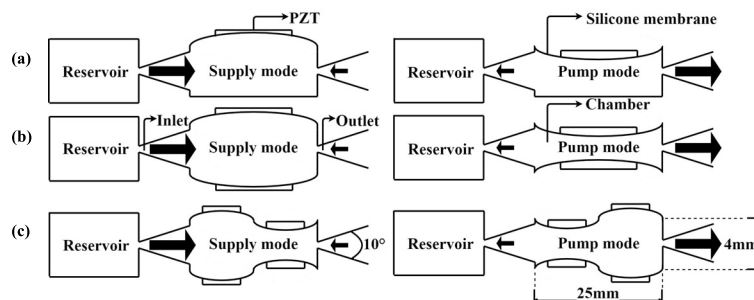

Fig. 2. The working principle of the proposed micropumps: (a) SDM, (b) BDM, and (c) PSM.

THEORETICAL ANALYSIS OF DIAPHRAGM

Our micropumps composed of four main components. These components include chamber, nozzle/diffuser elements, silicon membrane, and PZTs. By applying a positive voltage, PZT crystal is experiencing strain and by applying negative voltage, it is experiencing contraction. The silicon membrane is attached to the PZT edges. This has led to the creation of a mechanical vibration perpendicular to the silicon membrane.

The performance of PZT takes place in two stages, namely, the discharge and the suction. At discharge stage, a PZT actuator creates pressure on the silicon membrane. In this case, the silicon membrane bends towards the chamber. The volume of fluid carrier chamber will be reduced and the fluid will be directed out of the chamber. Fluid suction stage performance into the chamber takes place just after the completion of discharge stage. For suction, PZT actuator should move in the opposite direction. In other word, it must be bent upward. This causes the fluid in the reservoir to be sucked into the micropump chamber. To produce oscillatory flow, discharge and suction cycle will be repeated continuously in diaphragm micropump.

The PZT actuator, bonding layer, and the silicon membrane are three main components of diaphragm. We will call other silicon membrane parts that are not associated with the PZT as a free silicon membrane part. Bonding layer is an adhesive material that clamps the PZT actuator onto the silicon membrane.

Figure 3 shows the schematic of a single PZT layer micropump actuator. Analysis of the diaphragm displacement suggests that, in the free parts of silicon membrane, there will not be transverse or radial pressure and the potential energy for these parts will be the lowest. The neutral surface position can be obtained by using Equation (2) (Cui et al., 2008).
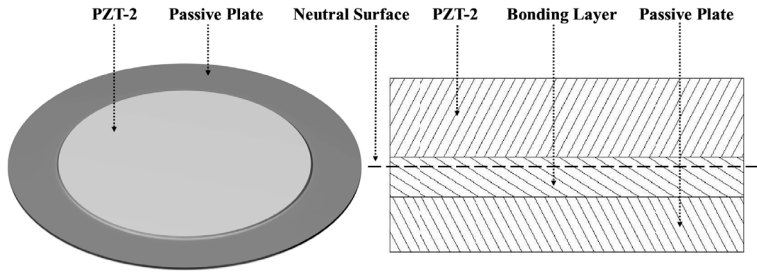
Fig. 3. Schematic of diaphragm component.

$$h = \frac{1}{2}\frac{(E_s h_s^2/(1-\gamma_s^2)) + (E_b[(h_b+h_s)^2 - h_s^2]/(1-\gamma_b^2)) + (E_{pzt}[(h_b+h_s+h_{pzt})^2 - (h_s+h_b)^2]/(1-\gamma_{pzt}^2))}{(E_s h_s/(1-\gamma_s^2)) + (E_b h_b/(1-\gamma_b^2)) + (E_{pzt}h_{pzt}/(1-\gamma_{pzt}^2))} \quad (2)$$

where "h" represents the thickness, "E" is Young's modulus and "γ" is Poisson's ratio, and the indices "s", "b", "pzt" express passive plate, bonding layer, and the piezo-ceramic. In micropump diaphragm, piezo-ceramic is attached to passive plate using the bonding layer. So, the three layers are concentric with each other and are created the piezoelectric actuator. At the time of the diaphragm vibration, the strain "ε" will be created in the three layers constantly. To ease the strain calculations, we will consider all three layers as equal and linear. The amount of displacement due to binding and concentric will be equal. But if displacement of all three layers will be measured of neutral surface, the amounts will not be identical. The stresses that occur in these layers can be calculated by using Equations (3-8) (Li et al., 2003). Here "z" is the amount of displacement form the neutral surface "k" is the slop of the strain, "σ_i" is the stress between the bonding layer and membrane, and "h" is the neutral surface distance from the bottom surface of the passive plate, the surface that directly is in contact with silicone diaphragm.

$$\sigma_b = \frac{E_b}{1-\gamma_b}\varepsilon_b \quad (3)$$

$$\varepsilon(z) = \varepsilon_p = \varepsilon_b = \varepsilon_{pzt} = kz \quad (4)$$

$$\sigma_s = \frac{\sigma_i}{h_p - h}z \quad (5)$$

$$k = \frac{1-\gamma_s}{E_s}\frac{\sigma_i}{h_s - h} \quad (6)$$

$$\sigma_b = \frac{E_b}{1-\gamma_b}kz = \frac{1-\gamma_s}{1-\gamma_b}\frac{E_b}{E_s}\frac{\sigma_i}{h_s-h}z \quad (7)$$

In this study, the diaphragm of micropumps vibrates at 5 Hz and 10 Hz. The frequencies that we used for diaphragm vibration were much lower than resonant frequency of PZT actuator. This is because we assume PZT actuator as isotropic elastic. Thereby, the stress–strain relationship can be expressed for PZT actuator.

$$\sigma_{pzt} = \frac{E_{pzt}}{1-\gamma_{pzt}}(kz - \frac{V}{h_{pzt}}d) = \frac{\sigma_i(1-\gamma_s)E_{pzt}}{(1-\gamma_{pzt})E_s(h_s-h)}z - \frac{E_{pzt}}{1-\gamma_{pzt}}\frac{V}{h_{pzt}}d \quad (8)$$

PZT shows interactions in electrical and mechanical behaviors. The governing equation on PZT mechanical deformation caused by the applied voltage can be calculated by using Equation (9) (He et al., 2017).

$$\varepsilon_{pzt} = s^E.\sigma_{pzt} + dE \quad (9)$$

where "s^E" is compliance tensor, "d" is constant tensor of PZT charge, and "E" is the electric field. The physical properties of PZT are given in Table 1. In addition, the silicon membrane properties can be summarized as Young's modulus (162 GPa), Poisson's ratio (0.22), and density (2329 kg/m³), respectively.

Table 1. PZT properties.

Property	Tensor (in order of x, y, z, xy, yz and xz)					
PZT stress tensor e (C/m²)	0	0	-1.81603			
	0	0	-1.81603			
	0	0	9.05058			
	0	9.77778	0			
	9.77778	0	0			
	0	0	0			
Elastic matrix C^E (N/m²)	13.48	6.78	13.48	0	0	0
	6.80	6.80	11.32	0	0	0
	0	0	0	0	0	0
	0	0	0	2.22	0	0
	0	0	0	0	2.22	0
	0	0	0	0	0	3.34
Compliance matrix (1/Pa)	11.6	-3.33	11.6	0	0	0
	-4.97	-4.97	1.48	0	0	0
	0	0	0	0	0	0
	0	0	0	45	0	0
	0	0	0	0	45	0
	0	0	0	0	0	29.9
Relative permittivity (F/m)	504.1	0	0			
	0	504.1	0			
	0	0	270			

THEORETICAL ANALYSIS OF MICROFLUIDIC

The analytical model that fluid mechanic theory provides for macroscopic flows can be used for the majority of micro-channels with larger than 1 μm in diameter. In this study, all dimensions are greater or equal to 200 μm. Only with the difference that the flow from laminar to the turbulent takes place at lower Reynolds Number (Peng et al., 1994). The net flow rate of micropump is associated with the hydrodynamic flow. One of the main reasons of energy waste in micro-channel is viscosity. Inertial effects also cause energy waste, but compared to other parameters, these effects are minimal. For this reason, we may ignore this issue. We considered our micro-channels with square cross-sectional areas, which creates Poiseuille flow. To calculate the loss of height in micro-channels, we used dimensional analysis Equations (10-11) of Darcy-Weisbach (Yunus et al., 2006). Consequently, we can calculate the net flow rate as Equation (12) (Yunus et al., 2006):

$$h_l = f \frac{l}{D_h} \frac{V^2}{2g} = \frac{64}{Re} \frac{l}{D_h} \frac{V^2}{2g} \tag{10}$$

$$P = \rho g h_l = \rho g \frac{64\mu l}{\rho V D_h^2} \frac{V^2}{2g} = \frac{32\mu l V}{D_h^2} \tag{11}$$

$$Q = \frac{\pi D_h^2}{4} V = \frac{\Delta P \pi D_h^2}{128\mu l} \tag{12}$$

where "h^l" is the loss of height in micro-channel, "P" is pressure, "f" is friction factor, "l" the length of micro-channel, "D_h" is diameter of micro-channel, "V" is average speed, "Re" is the Reynolds number of flow, "μ" is the viscosity coefficient, and "ρ" is density of the fluid.

The smallest characteristics of length of given micro-valves were 200 μm. In this case, the smallest characteristic of length is much larger than free scanning of water molecules. Water as the fluid is considered for pumping in the micropump because of the similar characteristics of eye drop. Knudsen number of water at ambient temperature conditions for the narrowest part of the micropump is equal to the 5^{-7} μm. Knudsen number can be calculated by using Equation (13) (Yunus et al., 2006).

$$Kn_{Water} = \frac{\lambda}{l_{min}} = \frac{10^{-4} \, \mu m}{200 \mu m} = 5^{-7} \, \mu m < 10^{-3} \tag{13}$$

where "Kn" is Knudsen number, "λ" free path of molecular, and "l_{min}" represents the length of smallest point of micro-channel. The obtained Knudsen number (5^{-7} μm < 10^{-3} μm) shows that the continuity condition is established for an incompressible fluid of water. So, for analysis of microfluidic behavior, we used Navier-Stokes equation. The wall thickness of micropump did not have any effect on the simulation results. Therefore, the specification of this parameter was ignored. We can apply a non-slip principle for micropump walls. The fluid in these areas will be static and non-animated. Given the dimension and geometry of the micropump, the emergence of high-speed is not possible for fluid. The range of Reynolds number for micro-channels is between 10 and 300.

BOUNDARY AND INITIAL CONDITIONS

In this study, it is assumed that there would be a laminar flow, incompressible and Newtonian fluid with constant properties. Therefore, we ignore volume forces. In order to solve the numerical flow, we used the Navier-Stokes steady flow equations (Yunus et al., 2006; Dereshgi et al., 2018). In Equations (14-15), "U" is fluid velocity; "x" is spatial direction. The "i" and "j" indices determine the coordinate directions in space.

$$\frac{\delta U_j}{\delta x_j} = 0 \tag{14}$$

$$\rho U_j \frac{\delta U_i}{\delta x_j} = -\frac{\delta P}{\delta x_i} + \mu \left(\frac{\delta^2 U_i}{\delta x_j \delta x_i} \right) \tag{15}$$

The boundary conditions are as follows: Along the ceiling and bottom walls of the microchannel, lateral walls of the chambers in BDM and PSM, and bottom and lateral walls of the chamber in SDM (fixed boundaries), the usual ''no slip'' boundary condition is prescribed for the fluid. The initial condition is zero for flow velocity and diaphragm displacements.

The operation pressure is 1 atm and the flow is assumed to be incompressible and laminar flow also flow properties are constant. Non-slip boundary conditions are thought to occur in the walls of the micropump. Controller equations show that the curvature of the membranes and the flow of liquid are always accompanied during the pumping operation. The law of conservation of momentum and continuity equation for incompressible fluids with Newtonian viscosity has taken place in the Navier-Stokes Equations (14-15).

STATISTICAL ANALYSES

Statistical analyses were performed in MATLAB 9.3. First, three measurements (displacement, flow rate, and fluid pressure) from each micropump design were averaged. Separate two-way ANOVAs were performed for the relevant variables: frequency and voltage. The factors in the ANOVAs were the frequency (5 Hz and 10 Hz) and voltage (5 V-45 V). Micropump data for voltage values were entered as repetitions. Multiple comparison test was used to compare displacement, flow rate, and fluid pressures.

RESULTS
FINITE ELEMENT ANALYSIS

In this study, the mesh convergence method was used to obtain satisfactory displacement amplitude of the diaphragm where the values saturated. By this method, it is possible to examine any parameter such as net flow and fluid pressure. According to the results, the displacement reached maximum at the center and zero at the edges. Clearly, diaphragm in supply mode (T/4) showed more displacement than pump mode (T/2). In contrast, we examined the diaphragm displacement in T/2 period, because the diaphragm applied maximum force to the fluid in this period. In addition to this, the analysis was done when the excitation input was at 5 V and 5 Hz to the PZT.

The analysis consists of four steps in the COMSOL Multiphysics 4.3 program. The four different types of meshes were selected. The number of meshes used in first step was less than the second step and this was repeated until the fourth step. The properties of the mesh are given in Table 2.

Table 2. Specifications of Finite Element Method (FEM).

Domain element statistics		Number of elements	Minimum element quality	Average element quality	Element area ratio	Mesh area (mm²)	Maximum growth rate	Average growth rate
SDM (250 µm)	Normal	9924	0.08612	0.8554	0.01369	128.6	3.544	1.341
	Fine	16517	0.126	0.8684	0.01977	128.6	3.518	1.239
	Finer	44068	0.1262	0.9013	0.00752	128.6	3.493	1.262
	Extra Fine	112955	0.1262	0.9196	0.00381	128.6	3.494	1.232
SDM (200 µm)	Normal	9976	0.08694	0.8535	0.01245	127.9	3.521	1.34
	Fine	16832	0.1255	0.8758	0.02373	127.9	3.547	1.256
	Finer	44268	0.1262	0.9006	0.00727	127.9	3.481	1.264
	Extra Fine	113730	0.1262	0.9196	0.00349	127.9	3.487	1.233
BDM	Normal	9767	0.1254	0.8505	0.01259	133.2	3.588	1.348
	Fine	15786	0.1272	0.8645	0.01951	133.2	3.519	1.257
	Finer	42861	0.1262	0.9013	0.00932	133.2	3.5	1.265
	Extra Fine	113635	0.1262	0.9231	0.00351	133.2	3.492	1.229
PSM	Normal	9781	0.1254	0.8505	0.01259	133.2	3.588	1.349
	Fine	15800	0.1272	0.8648	0.01951	133.2	3.519	1.257
	Finer	42895	0.1262	0.9013	0.00932	133.2	3.5	1.266
	Extra Fine	113669	0.13262	0.9231	0.00351	133.2	3.492	1.229

The error rates between the first meshing step (Normal) and the second meshing step (Fine) for the SDM with 250 µm PZT thickness, SDM with 200 µm PZT thickness, and BDM were 6.87 %, 3.25 %, and 8.29 %, respectively. For these three micropumps, the values were the very close at the second and subsequent steps. However, when we analyzed PSM's diaphragm, we obtained the result that the first and second steps were not appropriate according to the

error rate. Namely, there was a 19.42 % error between the first and the third steps (Finer mesh) and between the second and the third steps; this error fell to 7.69 %. In addition, there was no difference between the results of the third and the fourth steps. In the mesh convergence method, if the number of mesh elements is high, this increases the accuracy of the results. However, the analysis time will be highly increased. Therefore, we used the second step (Fine) mesh for the analysis of SDM (200 μm), SDM (250 μm), and BDM and the third step for analysis of PSM. The results of mesh convergence analysis were given in Figure 4.
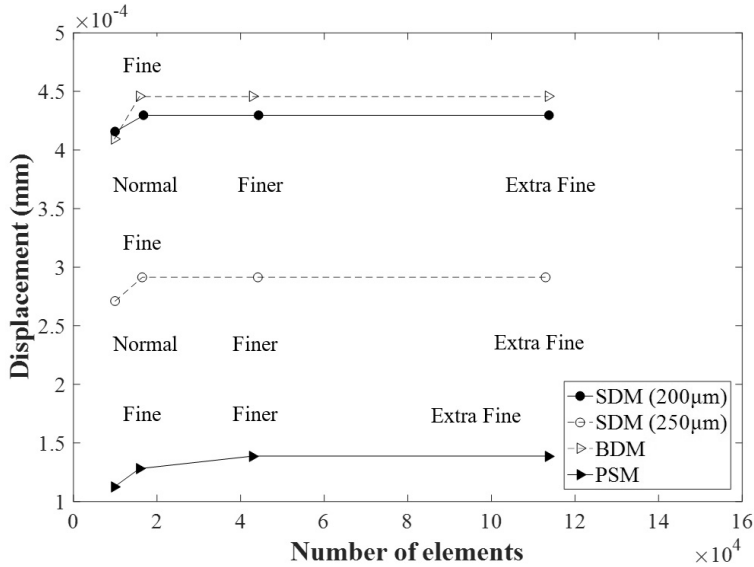
Fig. 4. Mesh convergence analysis for central point of micropumps' diaphragms.

BEHAVIOR OF DIAPHRAGMS

The results of four different models of micropump's diaphragm were obtained. The displacement results were given in Figure 5. According to these results, we can conclude that, by increasing the applied voltage, diaphragm displacement values will be increased. In other words, in all four micropumps, the maximum displacements of diaphragms took place at 45 V and the smallest displacements were at 5 V.

Firstly, the effect of the thickness of PZT actuation on the diaphragm deformation was studied. We analyzed the SDM and PZT with the thicknesses of 200 μm-250 μm and frequency of 5 Hz and 10 Hz in the mentioned voltage range. In the SDM, displacement values were slightly higher at 5 Hz than they were at 10 Hz for both diaphragm thicknesses. This is because the frequency of 5 Hz offers an opportunity to reach the maximum vibrating amplitude. The maximum displacements of this micropump with the PZT thicknesses of 250 μm in the frequencies of 5 Hz and 10 Hz were 2.50×10^{-3} mm and 2.44×10^{-3} mm. At the same voltage and frequency values, the maximum displacements of diaphragm for the PZT thickness of 200 μm were 3.50×10^{-3} mm and 3.42×10^{-3} mm. By comparing the obtained results, the amount of displacement created by PZT with 250 μm was less than a PZT with 200 μm thickness.

In the BDM, both diaphragms were vibrating with the same sinusoidal voltage, but in the opposite directions. While the upper diaphragm had the positive peak of the sinusoidal vibration, the lower diaphragm had the negative peak with a 180-degree phase shift. Because of the same voltage amplitude, the measured displacements for both diaphragms in this micropump were equal. The maximum displacements of this micropump for 5 Hz and 10 Hz frequencies were 3.68×10^{-3} mm and 3.50×10^{-3} mm and the minimum displacements were 4.46×10^{-4} mm and 3.90×10^{-4} mm, respectively. In the BDM, the pressure of the fluid inside the chamber from two directions was increased. In this case, the counterforce, in which the fluid affects the diaphragm, was reduced. Thereby, according to our simulation results, the amount of displacement of BDM was more than SDM.

The length of designed PZT for PSM was exactly half of the length of other PZT of micropump. The highest value for all 4 actuators was equal to 1.01×10^{-3} mm at 5 Hz. Statistical analyses showed that the PZT displacement values were significantly affected by the voltages (ANOVA, $p < 0.001$). In contrast, the frequency had moderate effect on displacement values for selected micropump designs (ANOVA, $p = 0.6244$). Multiple comparison analyses showed that maximum displacement was in BDM and was close to SDM with 200 μm PZT.
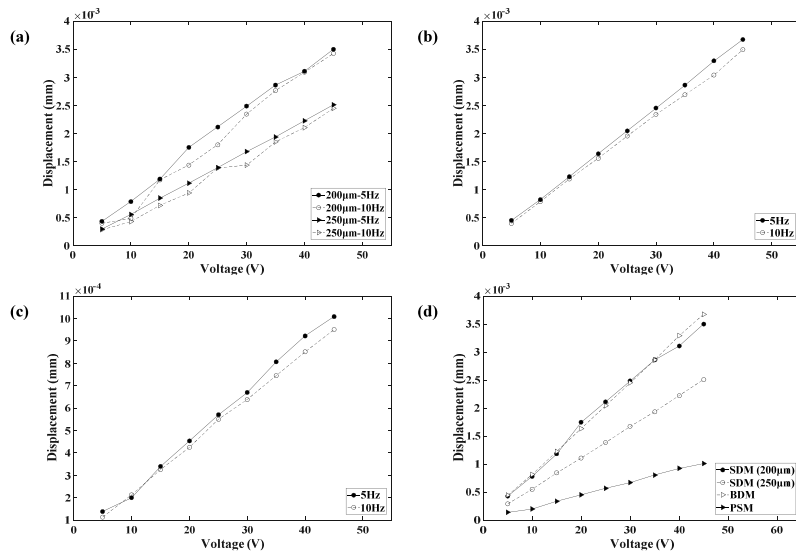
Fig. 5. The displacement results at 5 Hz-10 Hz: (a) SDM in different PZT thickness, (b) BDM, (c) PSM, and (d) Maximum displacement comparison of four micropumps.

FLOW RATES OF MICROPUMPS

Figure 6 shows the maximum obtained flow rate in the periods of diaphragms vibration during 3 seconds. The obtained results actually were related to the flow rate/cycle of the Equation (1). For the four-micropump design, we run simulations at 5 Hz and 10 Hz. The 5 Hz stimulation offers more flow rate/cycle for all voltages when compared to 10 Hz. However, the number of oscillations of the PZT in one direction at 10 Hz was doubled compared to 5 Hz. For this reason, the net flow rate during the period at 10 Hz was higher. The maximum obtained flow rates for SDM (250 μm), SDM (200 μm), BDM, and PSM at 5 Hz were 1.17×10^{-27} m³/cycle, 1.24×10^{-27} m³/cycle, 1.51×10^{-27} m³/cycle, and 1.62×10^{-27} m³/cycle, respectively. The maximum flow rates for SDM (250 μm), SDM (200 μm), BDM, and PSM at 10 Hz were 9.23×10^{-28} m³/cycle, 1.09×10^{-27} m³/cycle, 1.35×10^{-27} m³/cycle, and 1.39×10^{-27} m³/cycle, respectively. Statistical analyses showed that the effect of voltage on flow rate was significant (ANOVA, $p < 0.001$) and it was barely significant with the frequency (ANOVA, $p = 0.0465$).

Maximum flow rate values for SDM and PSM were at 45 V. As for BDM, it was at 30 V. In BDM, there were vortex and turbulence in the chamber of micropump higher than 30 V. In the laminar flow, the fluid particles pass regular and smooth routes so that each layer slowly slides on its adjacent layer. When two diaphragms from a different direction bend towards the chamber, high kinetic energy occurs in the particles of the fluid. In this case, when particles collide with each other, energy transfer occurs. Because of this reason, being higher than 30 V excitations, there was a decline in the flow rate in BDM.

Schematic of PSM was similar to BDM. The length of PZT of this micropump was half the length of BDM. The maximum displacement of diaphragm in this micropump was approximately one-third of the other micropumps. Therefore, the fluid inside the chamber moves in regular routes and creates laminar flow.
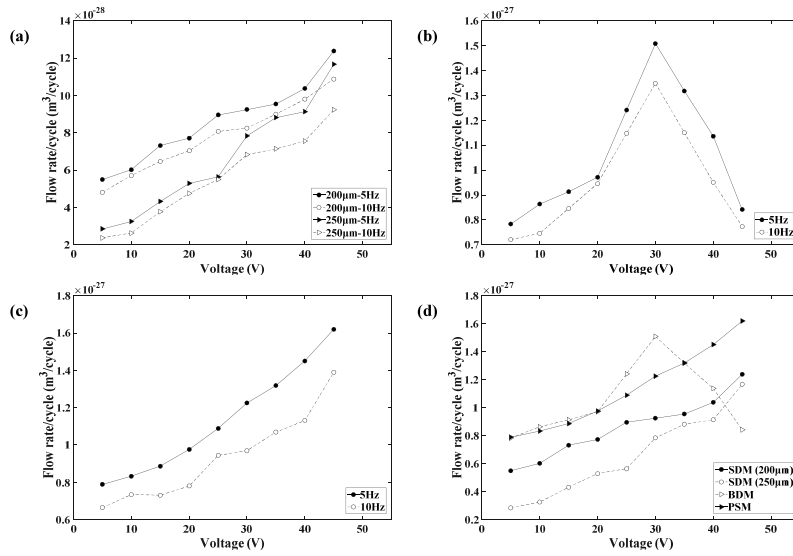
Fig. 6. The maximum flow rate results at 5 Hz-10 Hz: (a) SDM in different PZT thickness, (b) BDM, (c) PSM, and (d) Maximum flow rate comparison of four micropumps.

FLUID PRESSURE

The pressure was applied to the chamber's fluid by the diaphragm displacement. Figure 7 shows the maximum fluid pressure was obtained in the pumping mode. The graphic lines show the similar trend with the flow rate and fluid pressure. At all voltages, we calculated that the pressure values obtained at 5 Hz were higher than 10 Hz for the four micropumps. Figure 7.d shows the performance of all pumps for 5 Hz. BDM pressure values between all voltages between 5 V- 40 V were higher. The reason for this was the collection of pressures produced by the double diaphragm used in the design. After this value, pressure values were decreased, maybe due to the increased turbulence. According to Navier-Stokes equation, the direct relationship between pressure and flow rate also appeared in our results. In the statistical analyses, we found that fluid pressure levels were significantly affected by the voltage (ANOVA, $p < 0.001$) and frequency (ANOVA, $p = 0.0106$). Multiple comparison analysis showed that fluid pressure was higher for PSM design.
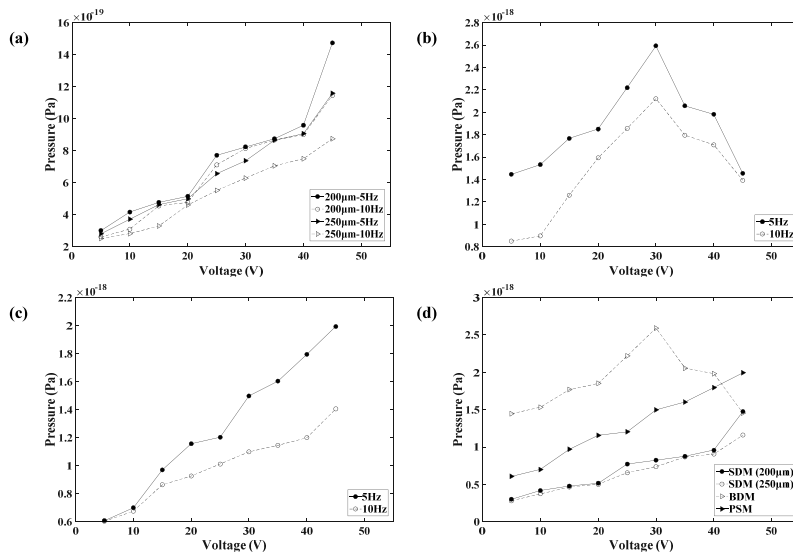

Fig. 7. The maximum fluid pressure results at 5 Hz-10 Hz: (a) SDM in different PZT thickness, (b) BDM, (c) PSM, and (d) Maximum fluid pressure comparison of four micropumps.

CONCLUSION

In this study, four novel micropumps, which may be used for the Glaucoma disease treatment, were designed. We studied the effects of electro-mechanical factors on the performance of micropump. It was found that the maximum displacement occurs at the central position of the diaphragm and the amount of displacement was dependent on the input voltage and PZT element thickness. The frequency showed moderate effect (ANOVA, p = 0.6244) when the PZT thickness was increased. Because the displacement of vibrating membrane would be reduced by the material. If the frequency and voltage will proportionally be increased, it will improve the performance and cause increment of pressure on micropump. In the simulation results, the flow rates were significantly different for each pump (ANOVA, p < 0.001) and were significantly changed by the frequency (ANOVA, p = 0.0565).

In the micropump with single diaphragm, the flow rate is limited. Thus, studies on multi-diaphragm micropumps are necessary. We can obtain characteristics like good stability, high flow rate, and high pressure in multi-diaphragm micropumps. In our study, the ideal voltage for BDM was 30 V. The higher voltage causes the higher displacement of diaphragm. The higher displacement from two sides will cause further pressure to the fluid of inside the chamber. Laminar flow of chamber turns to the turbulent flow. In this case, the micropump efficiency will be reduced. Hence, choosing the proper voltage has a significant impact on the performance of the micropump.

By comparing the change in the shape of PZT in the PSM and other PZT shapes in the provided study, reduction in the PZT displacement was observed. The simulation results indicate that the displacement of PZT depends on PZT's size.

In Glaucoma disease, eye drops should be suctioned from the anterior chamber of the eye. Because of the certain problems of the other fluid removal methods, micropumps can be considered one of the best useful devices. The behaviour of the micropumps depends on the fluid inside. In this study, we used water as fluid. In fact, the eye drops have different components from the water, which changes mechanical properties of the fluid. Even though there are some studies using water as fluid, the mechanical differences may significantly change the behaviour of the micropumps. This constitutes a limitation of our current study. After having the parameters about the eye drop, similar analyses will be applied in future studies.

COMPARISON WITH THE STATE OF THE ART

The flow rate of single chamber micropumps is limited due to the periodic vibration of the diaphragm. When the studies in Table 3 were investigated, it was seen that Afrasiab et al. (2011) and He et al. (2016) focused on increasing the limited flow rate of single chamber micropumps. Afrasiab et al. investigated the effects of a silicon diaphragm wave motion on the net flow rate by the finite element method. The upper ceiling wall of the chamber was covered with silicon diaphragm. Nine piezoelectric actuators were attached on the silicon diaphragm. The sinusoidal voltage was applied with $2\pi/3$ phase shift to piezoelectric actuators. Therefore, a peristaltic motion was applied to the fluid inside the chamber (Afrasiab et al., 2011). However, alternating pressures are the main factor of fluid motion. In their design, upper diaphragm was unable to apply pressure to the fluid in the bottom of the chamber. He et al. are focused on multi-chamber micropump. Consequently, their design created high flow rate compared to single chamber designs as expected (He et al., 2016). However, in their multi-chamber design, there was a turbulence, which is not preferred in micropump designs.
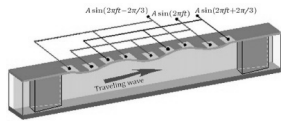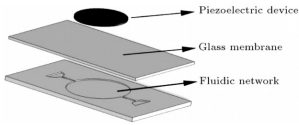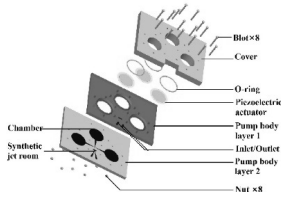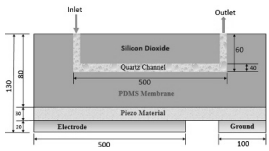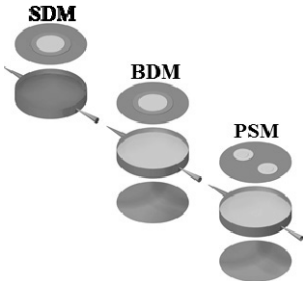
Kolahdouz et al. (2014) investigated the effects of different driving voltage shapes and frequencies on the diaphragm displacement and flow rate. In their study, they used a glass diaphragm, which has the thickness of 300 μm. However, the thickness of PZT actuator was 200 μm. Because of the stiffness of the glass material, relatively thin layer of PZT could not produce higher displacement values (~0.6 μm at 80 V). In our study, the displacement values of the diaphragm were almost 6 times higher (~3.6 in BDM) even though our driving voltage was 45 V. These results show the importance of the diaphragm and PZT actuator thickness selection in the micropump designs.

The flow rate is a key parameter and can be controlled by the vibration of the diaphragm, whereas our proposed configurations (BDM and PSM) consist of a chamber sandwiched between two diaphragms. Hereby, we have been

able to apply an alternative pressure to the fluid below the chamber. Thus, we improved the net flow rate with a simple geometric correction by two different micropump designs.

Sateesh et al. (2018) investigated the micro-channels diameter effects on flow velocity. In the study, polydimethylsiloxane (PDMS) membrane with thickness of 20 μm was placed on top of the piezoelectric actuator. Furthermore, 20 μm thick ground electrode and active electrode were placed under the piezoelectric actuator. Thereby, the piezoelectric actuator was compressed between two layers. As a result, this compression increases the resistance to piezoelectric vibration. The low vibration amplitude of the piezoelectric actuator may have caused the pressure at this micropump to be low. However, when SDM is compared with this micropump, the thickness of the silicon diaphragm (100 μm) in the SDM was about half of the thickness of the piezoelectric actuator (200 μm and 250 μm). Therefore, we achieved a high diaphragm displacement. Additionally, Sateesh et al. (2018) simulated micropump was very small in size. It might be very difficult and costly to fabricate, because it requires higher spatial resolution fabrication techniques, while the four micropumps in this study were simulated proportionally to the fabrication technology and commercially available materials.

Table 3. Comparison with the state of the art.

Ref.	Design Parameters	Figure	Explanation
Afrasiab et al., 2011	Valveless, nine PZT actuators, single chamber, silicone membrane.		Upper diaphragm was unable to apply pressure to the fluid in the bottom of the chamber.
Kolahdouz et al., 2014	Valveless, single PZT actuator, single chamber, glass membrane.		Low displacement values.
He et al., 2016	Valveless, three PZT actuators, three chambers, silicone membrane.		There was unwanted turbulence creating backpressure at output connection node.
Sateesh et al., 2018	Valveless, single PZT actuator, single chamber, PDMS membrane.		Very small channel size, very low flow rate.
Our work, 2019	SDM, BDM, PSM Valveless, PZT actuators, single chamber, silicone membrane.		High flow rates at low voltage and frequency. BDM and PSM have improved flow rates by double diaphragm on a single chamber, easy to produce by rapid prototyping due to sizes.

In the light of these findings, we may conclude that a PSM with four PZT elements might be a good candidate to be used in Glaucoma treatment in the clinics after further analyses and advanced fabrication technologies.

ACKNOWLEDGMENT

REFERENCES

Afrasiab, H., Movahhedy, M. R. & Assempour, A. 2011. Proposal of a new design for valveless micropumps. Scientia Iranica, **18**(6), 1261-1266.

Aggarwal, S., Paul, B. E., DasGupta, A. & Chatterjee, D. 2017. Experimental characterization of piezoelectrically actuated micromachined silicon valveless micropump. Microfluidics and Nanofluidics, **21**(1), 2.

Cobo, A., Sheybani, R., Tu, H. & Meng, E. 2016. A wireless implantable micropump for chronic drug infusion against cancer. Sensors and Actuators A: Physical, **239**, 18-25.

Cui, Q., Liu, C. & Zha, X. F. 2008. Simulation and optimization of a piezoelectric micropump for medical applications. The International Journal of Advanced Manufacturing Technology, **36**(5), 516-524.

Cui, Q., Liu, C. & Zha, X. F. 2008. Modeling and numerical analysis of a circular piezoelectric actuator for valveless micropumps. Journal of intelligent material systems and structures, **19**(10), 1195-1205.

De Moraes, C. G., Liebmann, J. M. & Levin, L. A. 2017. Detection and measurement of clinically meaningful visual field progression in clinical trials for glaucoma. Progress in retinal and eye research, **56**, 107-147.

Dereshgi, H. A. & Yildiz, M. Z. 2018. Investigation of electro-mechanical factors effecting piezoelectric actuator for valveless micropump characteristics. Journal of Engineering Science and Technology, **13**(9), 2843-2856.

Eladi, P. B., Chatterjee, D. & DasGupta, A. 2014. Design and development of a piezoelectrically actuated micropump for drug delivery application. In Micro and Smart Devices and Systems (pp. 127-141). Springer India.

Elder, M. J. 1994. Combined trabeculotomy-trabeculectomy compared with primary trabeculectomy for congenital glaucoma. British Journal of Ophthalmology, 78(10), 745-748.

Fan, B., Song, G. & Hussain, F. 2004, July. Simulation of a piezoelectrically actuated valveless micropump. In Smart Structures and Materials (pp. 126-134). International Society for Optics and Photonics.

Gensler, H., Sheybani, R., Li, P. Y., Mann, R. L. & Meng, E. 2012. An implantable MEMS micropump system for drug delivery in small animals. Biomedical microdevices, **14**(3), 483-496.

He, X., Xu, L., Zhang, X. & Yang, S. 2016. A bidirectional valveless piezoelectric micropump with three chambers applying synthetic jet. Journal of Mechanical Science and Technology, **30**(9), 4015-4022.

He, X., Xu, W., Lin, N., Uzoejinwa, B. B. & Deng, Z. 2017. Dynamics modeling and vibration analysis of a piezoelectric diaphragm applied in valveless micropump. Journal of Sound and Vibration, **405**, 133-143.

Jenke, C., Kager, S., Richter, M. & Kutter, C. 2018. Flow rate influencing effects of micropumps. Sensors and Actuators A: Physical, 276, 335-345.

Kawun, P., Leahy, S. & Lai, Y. 2016. A thin PDMS nozzle/diffuser micropump for biomedical applications. Sensors and Actuators A: Physical, **249**, 149-154.

Kolahdouz, E. M., Mohammadzadeh, K., Shirani, E. & Ziaei-Rad, S. 2014. Performance of piezoelectrically actuated micropump with different driving voltage shapes and frequencies. Scientia Iranica. Transaction B, Mechanical Engineering, **21**(5), 1635.

Lee, I., Hong, P., Cho, C., Lee, B., Chun, K. & Kim, B. 2016. Four-electrode micropump with peristaltic motion. Sensors and Actuators A: Physical, **245**, 19-25.

Li, S. & Chen, S. 2003. Analytical analysis of a circular PZT actuator for valveless micropumps. Sensors and Actuators A: Physical, **104**(2), 151-161.

Lloyd, A. W., Faragher, R. G. & Denyer, S. P. 2001. Ocular biomaterials and implants. Biomaterials, **22**(8), 769-785.

Ma, H. K., Chen, R. H., Yu, N. S. & Hsu, Y. H. 2016. A miniature circular pump with a piezoelectric bimorph and a disposable chamber for biomedical applications. Sensors and Actuators A: Physical, **251**, 108-118.

McMonnies, C. W. 2017. Glaucoma history and risk factors. Journal of optometry, **10**(2), 71-78.

Nisar, A., Afzulpurkar, N., Mahaisavariya, B. & Tuantranont, A. 2008. MEMS-based micropumps in drug delivery and biomedical applications. Sensors and Actuators B: Chemical, **130**(2), 917-942.

Nisar, A., Afzulpurkar, N., Tuantranont, A. & Mahaisavariya, B. 2008. Three dimensional transient multifield analysis of a piezoelectric micropump for drug delivery system for treatment of hemodynamic dysfunctions. Cardiovascular Engineering, **8**(4), 203-218.

Peng, X. F., Peterson, G. P. & Wang, B. X. 1994. Frictional flow characteristics of water flowing through rectangular microchannels. Experimental Heat Transfer An International Journal, **7**(4), 249-264.

Revathi, S. & Padmanabhan, R. 2018. Design and Development of Piezoelectric Composite-Based Micropump. Journal of Microelectromechanical Systems, **27**(6), 1105-1113.

Sateesh, J., Sravani, K. G., Kumar, R. A., Guha, K. & Rao, K. S. 2018. Design and flow analysis of MEMS based piezo-electric micro pump. Microsystem Technologies, **24**(3), 1609-1614.

Schuettauf, F., Quinto, K., Naskar, R. & Zurakowski, D. 2002. Effects of anti-glaucoma medications on gangion cell survival: the DBA/2J mouse model. Vision research, **42**(20), 2333-2337.

Shabanian, A., Goldschmidtboeing, F., Vilches, S., Phan, H. H., Kashekodi, A. B., Rajaeipour, P. & Woias, P. 2016. A novel piezo actuated high stroke membrane for micropumps. Microelectronic Engineering, **158**, 26-29.

Smits, J. G. 1990. Piezoelectric micropump with three valves working peristaltically. Sensors and Actuators A: Physical, **21**(1-3), 203-206.

Wang, Y. N. & Fu, L. M. 2018. Micropumps and biomedical applications–A review. Microelectronic Engineering, **195**, 121-138.

Yang, S., He, X., Yuan, S., Zhu, J. & Deng, Z. 2015. A valveless piezoelectric micropump with a Coanda jet element. Sensors and Actuators A: Physical, **230**, 74-82.

Yunus, A. C. & Cimbala, J. M. 2006. Fluid mechanics fundamentals and applications. International Edition, McGraw Hill Publication, New York, 185201.

تصميم وتحليل مضخات PZT مكروية للتطبيقات الطبية الحيوية: علاج الماء الأزرق

*مصطفى زاهد يلديز و**حميد اسدي درشجي

*قسم الهندسة الكهربائية والالكترونية، كلية التكنولوجيا، جامعة سكاريا للعلوم التطبيقية، تركيا

**هندسة الميكاترونيك، معهد العلوم الطبيعية، جامعة سكاريا، تركيا

الخلاصة

إن للمضخات الميكروية مجالاً واسعاً من التطبيقات الجديدة في المجال الطبي. لقد كان الهدف الرئيسي من هذه الدراسة هو إيجاد أبعاد التصميم الكهروميكانيكي المُحتمل للمضخات الميكروية لعلاج مرض الماء الأزرق. لقد اقترحنا أربعة تصاميم جديدة للمضخات الميكروية، هي: مضخات ميكروية أحادية الغشاء في سماكتين مختلفتين Piezoelectric ورصاص زيكرونات تيتانات (PZT-2). مضخات ميكروية ثنائية الغشاء ومضخات ذات الحركة الدودية. وكانت قيم جهد التشغيل في المحاكاة من 5 فولت إلى 45 فولت بمعدل زيادة 5 فولت وكان معدل التواتر 5 هرتز و10 هرتز. وأُجريت تحاليل ثنائية الأبعاد في برنامج COMSOL متعدد الفيزيائية 4.3. أُجريت أيضاً ثلاثة تحاليل تباين ANOVA مختلفة في اتجاه واحد لإيجاد تأثير الفولتاج (شدة التيار) والتكرار على معدلات التدفق. في معدلات تكرار مختلفة، كان هنالك فرق واسع في معدلات التدفق وضغط السائل ($p < 0.05$) من أجل جميع التصاميم للمضخة الميكروية. في قيم جهد تشغيل مختلفة، كان كل من الإزاحة، ضغط السائل ومعدل التدفق مختلفة إحصائياً ($p < 0.001$) لجميع المضخات الميكروية. كان معدل التدفق الأقصى الذي تم الحصول عليه في المضخة الميكروية 1.62×10^{-27} متر مكعب/ دورة. وكان أقصى إزاحة للغشاء حدثت في المضخات الميكروية ثنائية الغشاء 3.68×10^{-3} مم التي تم الحصول عليها في ظل قيمة جهد تبلغ 45 فولت وتردد 5 هرتز. بناءً على نتائجنا، تصميم المضخات الميكروية ذات الحركة الدودية يمكن استخدامها لعلاج مرض الماء الأزرق.